Beiträge aus der Elektrotechnik

Georg Meller

Energy-Efficient 434 MHz Wakeup Receivers Based on a Switched Passive Input Network With Surface Acoustic Wave Resonator

VOGT

Dresden 2025

Bibliografische Information der Deutschen Nationalbibliothek
Die Deutsche Nationalbibliothek verzeichnet diese Publikation in der Deutschen Nationalbibliografie; detaillierte bibliografische Daten sind im Internet über http://dnb.dnb.de abrufbar.

Bibliographic Information published by the Deutsche Nationalbibliothek
The Deutsche Nationalbibliothek lists this publication in the Deutsche Nationalbibliografie; detailed bibliographic data are available on the Internet at http://dnb.dnb.de.

Zugl.: Dresden, Techn. Univ., Diss., 2025

Die vorliegende Arbeit stimmt mit dem Original der Dissertation „Energy-Efficient 434 MHz Wakeup Receivers Based on a Switched Passive Input Network With Surface Acoustic Wave Resonator“ von Georg Meller überein.

Gesetzt vom Autor

ISBN 978-3-95947-083-4

Jörg Vogt Verlag
Niederwaldstr. 36
01277 Dresden
Germany

Phone: +49-(0)351-31403921
Telefax: +49-(0)351-31403918
e-mail: info@vogtverlag.de
Internet : www.vogtverlag.de

Technische Universität Dresden

Energy-Efficient 434 MHz Wakeup Receivers Based on a Switched Passive Input Network With Surface Acoustic Wave Resonator

Dipl.-Ing.
Georg Meller

der Fakultät Elektrotechnik und Informationstechnik
der Technischen Universität Dresden

zur Erlangung des akademischen Grades

Doktoringenieur
(Dr.-Ing.)

genehmigte Dissertation

Vorsitzender	Prof. Dr.-Ing. Dr. h.c. Gerhard Fettweis
Gutachter	Prof. Dr. sc. techn. habil. Frank Ellinger
Gutachter	Prof. Dr.-Ing. Dr.-Ing. habil. Robert Weigel

Tag der Einreichung	24.04.2025
Tag der Verteidigung	21.08.2025

Erklärung zur Autorenschaft

Hiermit versichere ich, dass ich die vorliegende Arbeit ohne unzulässige Hilfe Dritter und ohne Benutzung anderer als der angegebenen Hilfsmittel angefertigt habe; die aus fremden Quellen direkt oder indirekt übernommenen Gedanken sind als solche kenntlich gemacht. Bei der Auswahl und Auswertung des Materials sowie bei der Herstellung des Manuskripts habe ich Unterstützungsleistungen von folgenden Personen erhalten: Prof. Dr.-Ing. habil. Frank Ellinger und Dr. Jens Wagner.

Weitere Personen waren an der geistigen Herstellung der vorliegenden Arbeit nicht beteiligt. Insbesondere habe ich nicht die Hilfe eines kommerziellen Promotionsberaters in Anspruch genommen. Dritte haben von mir weder unmittelbar noch mittelbar geldwerte Leistungen für Arbeiten erhalten, die im Zusammenhang mit dem Inhalt der vorgelegten Dissertation stehen.

Die Arbeit wurde bisher weder im Inland noch im Ausland in gleicher oder ähnlicher Form einer anderen Prüfungsbehörde vorgelegt und ist auch noch nicht veröffentlicht worden. Mir ist bekannt, dass die Nichteinhaltung dieser Erklärung zum nachträglichen Entzug des Doktortitels führen kann.

Ich bestätige, dass ich die Promotionsordnung der Fakultät Elektrotechnik und Informationstechnik vom 08. August 1994 in der geänderten Fassung 12.05.2012 und die Änderungssatzung vom 18.06.2018 der Technischen Universität Dresden anerkenne.

Dresden, April 2025

Georg Meller

Danksagung

Zuerst möchte ich Prof. Dr. sc. techn. habil. Frank Ellinger danken für die Möglichkeit, meine Dissertation an der Professur für Schaltungstechnik und Netzwerktheorie anzufertigen, für die Betreuung der Arbeit, das entgegengebrachte Vertrauen und für das Korrekturlesen. Prof. Dr.-Ing. Dr.-Ing. habil. Robert Weigel danke ich dafür, dass er als externer Gutachter fungiert hat. Dr. Jens Wagner möchte ich danken für die angenehme Betreuung innerhalb der Arbeitsgruppe, fachlichen Austausch, wertvolles Feedback und Korrekturlesen. Dr. Michael Methfessel gilt mein Dank für zahllose Diskussionen und die konstruktive Zusammenarbeit über die letzten Jahre hinweg. Dr. Stefan Schumann danke ich für Lehrstuhl- und Laborverwaltung. Bei Frau Isaack bedanke ich mich für Hilfe und Unterstützung bei Formalien und bürokratischen Vorgängen. Dr. Chris Hoyer und Dr. Xin Xu möchte ich meinen Dank aussprechen für Unterstützung mit der Dokumentenvorlage. Florian Protze und Maximilian Froitzheim gilt mein herzlicher Dank für mühevolle Bondarbeiten der zahlreichen zweireihigen Chip-Pads. Frank Bindrich und Florian Protze danke ich für IT Unterstützung. Dr. Tilo Meister danke ich für die Unterstützung bei diversen Tapeouts. Max Becker möchte ich für ein angenehmes und produktives Büroklima danken. Lucas Ott, Helmuth Morath und Yizhou Xu danke ich für Unterstützung bei den Übertragungsexperimenten. Dr. Simon Buhr danke ich für sein großartiges Schaltplan Zeichenprogramm. Allen Kollegen danke ich für die kollegiale Arbeitsatmosphäre, Unterstützung und vielen hilfreichen Diskussionen.

Dem *Leibniz-Institut für Festkörper- und Werkstoffforschung Dresden* (IFW) sowie Frau Dr. Alejandra M. Castro Chong danke ich für die Herstellung und Bereitstellung der Perowskit-Solarzellen.

GlobalFoundries danke ich für die Fabrikation von Chips im Rahmen des "University Partnership Program".

Einen großen Dank möchte ich meiner Familie aussprechen, besonders meinen Eltern und Großeltern, welche mich immer unterstützt haben. Meinem Bruder und meinem Großvater danke ich für den Zuspruch bei der Entscheidung für eine Promotion. Yizhou Xu danke ich für Unterstützung, Verständnis und Empathie.

Abstract

Wakeup receivers (WuRxs) are a key enabler for energy efficient wireless communication and sensor networks. They are intended to receive a wakeup sequence (WUS) to wake up a wireless node subsequently. This class of wireless receivers (Rxs) need to exhibit a sufficient input sensitivity and input filtering bandwidth at very low direct current (dc) power consumption, which are typically below 1 µW. The requirements on the data rate are relaxed, depending on the tolerable wakeup latency. On the other hand, a WuRx can also be used to receive payload data, if low data rates are sufficient.

This work proposes two novel on-off keying (OOK) WuRx architectures operating in the 434 MHz industrial, scientific and medical (ISM) band, namely the *switched passive input network (SPIN) amplifier Rx* and the *switched injection-triggered oscillator (SITO) Rx*. They both rely on a novelly proposed *SPIN* based on a cheap (1$) commercial off-the-shelf (COTS) surface acoustic wave (SAW) resonator. It is shown that this off-chip surface mounted device (SMD) component adds very little to the Rx system size, which is typically dominated by the antenna for Rxs operating at this carrier frequency. For the SPIN output voltage, an analytical transient description is derived for varying loss resistances. It turns out, that the loss resistance is dominated by the losses in the off-chip inductor.

The *SPIN amplifier Rx* can be categorized as a direct radio frequency (RF) demodulation Rx, characterized by the SPIN instead of a conventional steady state input matching network (IMN). A SPIN amplifier Rx prototype comprising the analog frontend (AFE) and a digital backend (DBE) is implemented in IHP SGB25V 250 nm bipolar CMOS (BiCMOS) technology.

The *SITO Rx* on the other hand poses a promising alteration of the super-regenerative receiver (SRR), by injecting the input signal into the oscillator via the SAW resonator, which is part of the SPIN. A noise model for the SITO, which is an oscillator with two resonators and thus two oscillation frequencies, is derived in this work. This noise model is based on the noise analysis for a single resonator super-regenerative amplifier (SRA) found in the literature. The noise model is validated against measurements of a proof-of-concept Rx implemented in GlobalFoundries 22 nm fully depleted silicon on insulator (FD-SOI) technology. The dc power consumption and the input sensitivity of the SITO Rx both are limited by the losses in the off-chip inductor of the SPIN. It is shown by calculations and measurements of a proof-of-concept Rx system, that the SITO Rx behaves conversely compared to the SRR in terms of input sensitivity vs. oscillator ramp-up

time. Furthermore, the SITO Rx makes the input frequency selectivity largely independent of the ramp-up length. Another implementation in GlobalFoundries 22 nm FD-SOI technology achieves a very performant combination of good input sensitivity, i.e., −94 dBm (BER $\leq 10^{-3}$), a narrow input 3 dB bandwidth (BW) of only 133 kHz and a very low consumed dc energy per bit of the AFE of only $E_b = 2.8$ pJ (all measured). Based on the assumption, that the dc energy consumption of a wireless Rx is dominated by the AFE, this corresponds to a reduction of the consumed dc energy per bit by a factor of 138 compared to state-of-the-art (SOTA) Rxs. This results in a low average dc power consumption, e.g., 28 nW from a 0.3 V and 0.8 V supply at a data rate of 10 kbps.

This high energy efficiency of the wireless Rx opens up new possibilities in terms of batteryless wireless internet of things (IoT) nodes, since this low dc power can be provided from energy harvesting solutions with only small geometrical size. This is proven by supplying an Rx AFE presented in this work from two Perovskite solar cells with an area of only 9 mm^2 in total, while at the same time enabling sufficient transmission distances of over 100 m.

Kurzfassung

Aufwachempfänger sind eine Schlüsselkomponente für die Realisierung energieeffizienter drahtloser Kommunikations- und Sensornetze. Die Aufgabe des Aufwachempfängers besteht darin, eine Aufwachnachricht drahtlos zu empfangen, um den drahtlosen Knoten anschließend aufzuwecken. Diese Klasse von Drahtlosempfängern muss eine suffiziente Eingangsempfindlichkeit und eingangsseitige 3 dB-Bandbreite aufweisen bei einer sehr geringen durchschnittlichen DC-Leistungsaufnahme, welche typischerweise unter 1 µW liegt. Die Anforderungen an die Datenrate hingegen sind vergleichsweise gering, abhängig von der tolerierbaren Aufwachlatenz.

Diese Arbeit schlägt zwei neuartige Architekturen für Aufwachempfänger vor, welche ein-aus getastete (engl. *on-off keying (OOK)*) Signale auf einer Trägerfrequenz im 434 MHz ISM-Band empfangen können: der Empfänger mit geschaltetem passiven Eingangsnetzwerk (engl. *switched passive input network (SPIN)*) samt Verstärker und der geschaltete injektionsausgelöste Oszillator (engl. *switched injection-triggered oscillator (SITO)*) -Empfänger. Beide basieren auf dem neuartig vorgeschlagenen geschalteten passiven Eingangsnetzwerk, welches einen günstigen (1$) kommerziell erhältlichen akustischen Oberflächenwellen (engl. *surface acoustic wave (SAW)*) -Resonator nutzt. Es wird gezeigt, dass dieses oberflächenmontierte Bauteil, welches nicht Teil des Chips ist, die Größe des Empfängersystems nur marginal erhöht, da die Systemgröße bei dieser Trägerfrequenz üblicherweise von der Größe der Antenne dominiert wird. Für die Ausgangsspannung des SPINs wird eine analytische Beschreibung im Zeitbereich für verschiedene Verlustwiderstände hergeleitet. Es zeigt sich, dass der Verlustwiderstand durch die Verluste in der externen Spule dominiert wird.

Der Empfänger mit SPIN samt Verstärker kann klassifiziert werden als Empfänger mit direkter Hochfrequenz (HF) Demodulation (auch *Geradeausempfänger* genannt), wobei das Eingangsanpassungsnetzwerk für stationärem Betrieb durch das oben genannte SPIN ersetzt wird. Ein Empfängersystem mit SPIN und Verstärker wurde in IHP SGB25V 250 nm BiCMOS Technologie implementiert, bestehend aus analogem Frontend und Digitalteil.

Andererseits stellt der SITO-Empfänger eine Abwandlung des Superregenerativempfängers (engl. *super-regenerative receiver (SRR)*) dar, bei der die Signalinjektion in den Oszillator über den SAW-Resonator erfolgt, welcher Teil des SPINs ist. In dieser Arbeit wird ein Rauschmodell für den SITO hergeleitet, welcher einen Oszillator mit zwei Resonatoren und daher mit zwei

Oszillationsfrequenzen darstellt. Diese Rauschmodell basiert auf der Rauschanalyse eines superregenerativen Verstärkers mit einem einzelnen Resonator aus der Literatur. Das Rauschmodell wird mit Hilfe von Messungen eines Empfängerprototyps validiert, welcher in GlobalFoundries 22 nm FD-SOI Technologie implementiert wurde. Die DC-Leistungsaufnahme sowie die Eingangsempfindlichkeit des SITO-Empfängers werden beide limitiert durch die Verluste in der externen Spule des SPINs. Anhang von Berechnungen und Messungen eines Empfängerprototyps wird gezeigt, dass der SITO-Empfänger sich konträr zum SRR verhält hinsichtlich Eingangsempfindlichkeit in Abhängigkeit von der Anschwingzeit des Oszillators. Darüber hinaus ist die eingangsseitige Frequenzselektivität des SITO-Empfängers weitgehend unabhängig von der Anschwingzeit. Ein weiterer Empfängerprototyp implementiert in GlobalFoundries 22 nm FD-SOI Technologie erreicht eine leistungsfähige Kombination von guter Eingangsempfindlichkeit (−94 dBm bei einer Bitfehlerrate von maximal 10^{-3}), einer schmalen eingangsseitigen 3 dB-Bandbreite von lediglich 133 kHz und einer sehr geringen DC-Energieaufnahme des analogen Frontends je Bit von nur $E_\mathrm{b} = 2.8\,\mathrm{pJ}$ (all diese Werte wurden gemessen). Ausgehend von der Annahme, dass die DC-Leistungsaufnahme eines Drahtlosempfängers vom analogen Frontend dominiert wird, erzielt der SITO-Empfänger eine Reduktion der DC-Leistungsaufnahme je Bit um einen Faktor 138 gegenüber Drahtlosempfängern gemäß Stand der Technik. Das resultiert in einer sehr geringen durchschnittlichen DC-Leistungsaufnahme, beispielsweise von 28 nW von einer 0.3 V und einer 0.8 V Versorgungsspannung bei einer Datenrate von 10 kbps.

Diese hohe Leistungseffizienz des Drahtlosempfängers eröffnet neue Möglichkeiten in Hinblick auf batterielose drahtlose Knoten für das Internet der Dinge (engl. *internet of things (IoT)*), da die benötigte DC-Leistung bereitgestellt werden kann von kompakten Modulen zur Energiegewinnung (engl. *energy harvesting*). Dies wird nachgewiesen durch den Betrieb eines hier vorgestellten analogen Empfängerfrontends von zwei Perowskit-Solarzellen mit einer Gesamtfläche von $9\,\mathrm{mm}^2$, während gleichzeitig eine Übertragungsdistanz von mehr als 100 m gezeigt wird.

List of Abbreviations

ac	alternating current
ACF	autocorrelationfunction
ADC	analog-to-digital converter
AE	active element
AFE	analog frontend
AGC	automatic gain control
AM	amplitude modulation
ASIC	application-specific integrated circuit
ASK	amplitude-shift keying
BAW	bulk acoustic wave
BB	baseband
BE	bit error
BER	bit error rate
BiCMOS	bipolar CMOS
BLDC	bit-level duty-cycling
BJT	bipolar junction transistor
BP	bandpass
BPF	band-pass filter
BVD	Butterworth–Van-Dyke
BW	bandwidth
CD	common-drain
CE	code error
CER	code error rate
CMOS	complementary metal-oxide-semiconductor
COB	chip on board
COTS	commercial off-the-shelf
CPSD	cross power spectral density
CS	common-source
CW	continuous wave
DAC	digital-to-analog converter
DBE	digital backend
dc	direct current
D-FF	data flip-flop
DMM	digital multimeter
DOF	degree of freedom
ED	energy detector
ENBW	equivalent noise bandwidth
ESD	energy spectral density

FD-SOI	fully depleted silicon on insulator
FOM	figure of merit
FRAM	ferroelectric random access memory
FSK	frequency shift keying
FVF	flipped voltage follower
HB	harmonic balance
HBT	heterojunction bipolar transistor
HPF	high-pass filter
iid	independent and identically distributed
ISI	intersymbol interference
IF	intermediate frequency
IC	inversion coefficient
ICT	information and communications technology
IMN	input matching network
IoT	internet of things
IQ	in-phase and quadrature
ISM	industrial, scientific and medical
LDO	low dropout regulator
LED	light-emitting diode
LNA	low noise amplifier
LO	local oscillator
LPF	low-pass filter
LSB	least significant bit
LTI	linear time-invariant
LTV	linear time-variant
MEMS	micro-electromechanical system
MCU	microcontroller unit
MOM	metal-oxide-metal
MOS	metal-oxide-semiconductor
MOSFET	metal-oxide-semiconductor field-effect transistor
MS	mean square
NFET	n-channel MOSFET
NRZ	non-return-to-zero
OOK	on-off keying
OP	operating point
OTA	operational transconductance amplifier
PCB	printed circuit board
PDF	probability density function
PDK	process design kit
PLDC	packet-level duty-cycling
PFET	p-channel MOSFET
PG	processing gain
PLE	path loss exponent

PLL	phase-locked loop
PMF	probability mass function
PN	phase noise
PRBS	pseudorandom binary sequence
PSD	power spectral density
PVT	process, voltage and temperature
RF	radio frequency
Rx	receiver
RV	random variable
SAW	surface acoustic wave
SIR	signal-to-interference ratio
SITO	switched injection-triggered oscillator
SMD	surface mounted device
SNR	signal-to-noise ratio
SOTA	state-of-the-art
SOI	silicon on insulator
SPI	serial peripheral interface
SPIN	switched passive input network
SRA	super-regenerative amplifier
SRF	self-resonant frequency
SRR	super-regenerative receiver
ssec	small-signal equivalent circuit
TE	transistor efficiency
TEC	thermoelectric cooler
TEG	thermoelectric generator
TI	time-invariant
TV	time-varying
Tx	transmitter
UG	unity gain
VCO	voltage-controlled oscillator
VNA	vector network analyzer
WPDC	within-packet duty-cycling
WuRx	wakeup receiver
WUS	wakeup sequence

List of Symbols

Mathematical and Physical Constants

Symbol	Value	Unit	Description
π	3.142	1	circle number
c_0	$299.8 \cdot 10^6$	m/s	speed of light in vacuum
e	2.718	1	Euler's number
j	$\sqrt{-1}$	1	imaginary unit
k	$1.381 \cdot 10^{-23}$	J/K	Boltzmann constant
q	$1.602 \cdot 10^{-19}$	C	elementary charge

Quantities

Symbol	Unit	Description
$\alpha(t)$	1/s	overall exponential decay/growth rate of a resonator
α_1	1/s	$\alpha(t)$ during phase 1
α_2	1/s	$\alpha(t)$ during phase 2
α_{L2C2}	1/s	exponential decay/growth rate of the L_2C_2 tank itself
β	1/s	ramp slope of a ramp controlled SRR
γ	1	MOSFET thermal channel noise current coefficient
γ_0	1	technology constant for normalizing γ
γ_{SRR}	1	parameter of a ramp controlled SRR relating ramp length t_b and ramp slope β to each other
δ	1	Dirac delta function
$\tan(\delta)$	1	loss tangent of a printed circuit board (PCB) substrate
ϵ	1	time domain stretch factor of $g(t)$ of an SRR
$\zeta(t)$	1	damping ratio of a resonator
ζ_1	1	$\zeta(t)$ during phase 1

Symbol	Unit	Description
ζ_2	1	$\zeta(t)$ during phase 2
λ	m	wavelength
$\mu(t)$	1	normalized envelope of an SRA
$\mu_{1,\mathrm{f1}}(t)$	1	$\mu_{\mathrm{f1}}(t)$ during phase 1
$\mu_{1,\mathrm{f2}}(t)$	1	$\mu_{\mathrm{f2}}(t)$ during phase 1
$\mu_{2,\mathrm{f1}}(t)$	1	$\mu_{\mathrm{f1}}(t)$ during phase 2
$\mu_{2,\mathrm{f2}}(t)$	1	$\mu_{\mathrm{f2}}(t)$ of $V_{\mathrm{SAW,f2}}(t)$ during phase 2
$\mu_{\mathrm{f1}}(t)$	1	normalized envelope of $V_{\mathrm{SAW,f1}}(t)$
$\mu_{\mathrm{f2}}(t)$	1	normalized envelope of $V_{\mathrm{SAW,f2}}(t)$
ρ	1	correlation coefficient
σ_{s}	s	SRA time constant
σ_{X}	A	standard deviation of real and imaginary part of the complex phasor $\underline{X}(\omega_0)$
$\sigma_{\mathrm{X,f1}}$	A	standard deviation of real and imaginary part of the complex phasor $\underline{X}(\omega_1)$
$\sigma_{\mathrm{X,f2}}$	A	standard deviation of real and imaginary part of the complex phasor $\underline{X}(\omega_2)$
τ	s	time constant of a first-order linear time-invariant (LTI) system
ϕ_{a}	rad	phase of SRA injection current
ϕ_{S}	rad	signal phase
ω	rad/s	angular frequency
ω_0	rad/s	angular resonance frequency of the SAW resonator $\omega_0 = 2\pi f_0$
ω_1	rad/s	angular resonance of first SPIN resonance mode $\omega_1 = 2\pi f_1$
ω_2	rad/s	angular resonance of second SPIN resonance mode $\omega_2 = 2\pi f_2$
ω_{a}	rad/s	angular frequency of the SRA injection current $\omega_{\mathrm{a}} = 2\pi f_{\mathrm{a}}$
ω_{sig}	rad/s	angular frequency of a signal
Ω_{s}	1/s	SRA frequency constant
$A_{\mathrm{V,pulse}}$	1	pulse voltage gain of the SPIN
$A_{\mathrm{V,pulse,ideal}}$	1	pulse voltage gain of the lossless SPIN
BER	1	bit error rate (BER)

Symbol	Unit	Description
BW_0	Hz	reference noise $\mathrm{BW}_{\mathrm{noise}}$
$\mathrm{BW}_{\mathrm{3dB}}$	Hz	RF 3 dB BW
$\mathrm{BW}_{\mathrm{BB,3dB}}$	Hz	baseband (BB) 3 dB BW: $\mathrm{BW}_{\mathrm{BB,3dB}} = \mathrm{BW}_{\mathrm{3dB}}/2$
$\mathrm{BW}_{\mathrm{noise}}$	Hz	noise BW
$\mathrm{BW}_{\mathrm{rel}}$	1	relative BW
C_1	F	motional capacitance of the SAW resonator Butterworth–Van-Dyke (BVD) model
C_2	F	total shunt capacitance C_2
$C_{2,\mathrm{rest}}$	F	remaining shunt capacitance; part of C_2
$C_{2,\mathrm{stray}}$	F	PCB stray capacitance; part of C_2
$C_{2,\mathrm{SAW}}$	F	shunt capacitance of the SAW resonator BVD model; part of C_2
$C_{2,\mathrm{tune}}$	F	tuning capacitance; part of C_2
C_{ac}	F	alternating current (ac) coupling capacitor
C_{FB}	F	feedback capacitance
C_{GS}	F	gate-source capacitance
C_{i}	1	i-th bit of the code
C_{L}	F	load capacitance
C_{par}	F	parasitic substrate capacitance
CER	1	code error rate (CER)
Corr	1	correlator output, which is a discrete random variable (RV)
$\mathrm{Corr}_{\mathrm{A}}$	1	Corr, if no code is sent from the transmitter (Tx)
$\mathrm{Corr}_{\mathrm{A0}}$	1	$\mathrm{Corr}_{\mathrm{A}}$ summand for $C_{\mathrm{i}} = 0$
$\mathrm{Corr}_{\mathrm{A1}}$	1	$\mathrm{Corr}_{\mathrm{A}}$ summand for $C_{\mathrm{i}} = 1$
$\mathrm{Corr}_{\mathrm{B}}$	1	Corr, if a code is sent from the Tx
$\mathrm{Corr}_{\mathrm{B0}}$	1	$\mathrm{Corr}_{\mathrm{B}}$ summand for $C_{\mathrm{i}} = 0$
$\mathrm{Corr}_{\mathrm{B1}}$	1	$\mathrm{Corr}_{\mathrm{B}}$ summand for $C_{\mathrm{i}} = 1$
$\mathrm{Corr}_{\mathrm{thresh}}$	1	correlator output threshold
d	m	wireless transmission distance
D	1	duty-cycle ratio

Symbol	Unit	Description
$\mathrm{DAC_{CMP}}$	1	digital-to-analog converter (DAC) word setting the comparator threshold
$\mathrm{DAC_{CMP,opt}}$	1	DAC word for optimum input sensitivity
E_b	J	consumed dc energy per bit
$E_\mathrm{b,AFE}$	J	dc energy per bit consumed by the AFE
$E_\mathrm{b,osc}$	J	dc energy per bit consumed by the oscillator
$E_\mathrm{b,osc,settle}$	J	dc energy per bit consumed by the oscillator during turn-on settling
$E_\mathrm{b,osc,sample}$	J	dc energy per bit consumed by the oscillator for ramp-up and sampling
E_g	s	energy of the sensitivity function $g(t)$
E_g1	s	energy of the sensitivity function $g(t)$ in phase 1
E_g2	s	energy of the sensitivity function $g(t)$ in phase 2
$E_\mathrm{g,tran}(t)$	s	accumulation term converging against E_g
ENBW	Hz	equivalent noise BW
f	Hz	frequency of a wireless signal
Δf	Hz	frequency offset of an interferer
f_0	Hz	resonance frequency of the SAW resonator or signal frequency
f_1	Hz	first SPIN resonance frequency/mode
f_2	Hz	second SPIN resonance frequency/mode
f_a	Hz	frequency of the SRA injection current
f_AM	Hz	SPIN amplitude modulation (AM) frequency: $f_\mathrm{AM} = (f_2 - f_1)/2$
f_hi	Hz	higher bound of frequency interval
f_in	Hz	input frequency
f_lo	Hz	lower bound of frequency interval
f_sampling	Hz	sampling frequency
$\mathrm{FOM_{dB}}$	dB	figure of merit (FOM) in dB-scale associated with $P_\mathrm{in,sens,dBm}$ ($\mathrm{BER} \leq 10^{-3}$)
$g(t)$	1	sensitivity function of an SRA, associated with $\mu(t)$

Symbol	Unit	Description
$\tilde{g}(t)$	1	modified version of the sensitivity function $g(t)$ after applying the time domain stretch factor ϵ
$g_1(t)$	1	sensitivity function of an SRA during phase 1
$g_2(t)$	1	sensitivity function of an SRA during phase 2
g_m	S	transconductance of a transistor
g_m1	S	transconductance of first operational transconductance amplifier (OTA) stage
g_m2	S	transconductance of second OTA stage
G	S	conductance $G = 1/R$
$\underline{G}(\omega)$	s	Fourier transform of $g(t)$
$\underline{G}_1(\omega)$	s	Fourier transform of $g_1(t)$
$\underline{G}_2(\omega)$	s	Fourier transform of $g_2(t)$
$\underline{G}_\mathrm{HPF}(j\omega)$	1	transfer function of a high-pass filter (HPF)
G_loss	S	total parallel loss conductance of the SPIN: $G_\mathrm{loss} = 1/R_\mathrm{loss}$
G_L2C2	S	total parallel conductance of the SPIN, including G_osc
G_osc	S	negative conductance due to active element (AE) of oscillator, which contributes to G_L2C2 of the SPIN
G_Rx	1	Rx antenna gain in linear scale
$G_\mathrm{Rx,dBi}$	dBi	Rx antenna gain in dB-scale
G_Tx	1	Tx antenna gain in linear scale
$G_\mathrm{Tx,dBi}$	dBi	Tx antenna gain in dB-scale
h	m	thickness of a layer in a PCB stack-up
$\underline{H_\mathrm{b}}(j\omega)$	1	transfer function of bias network
$\underline{H_\mathrm{charge}}(j\omega)$	1	transfer function from V_source to V_C1
$i_\mathrm{a}(t)$	A	SRA injection current
$i'_\mathrm{a}(t)$	A	SRA injection current time derivative $i'_\mathrm{a} = \frac{d}{dt} i_\mathrm{a}(t)$
$i_\mathrm{source}(t)$	A	current of Norton equivalent current source
$\hat{I}$	A	amplitude of sinusoidal current I
I_0	A	technology MOSFET current constant

Symbol	Unit	Description
I_1	A	dc operating point (OP) current of first amplifier stage
I_2	A	dc OP current of second amplifier stage
I_{avg}	A	average current consumption from dc supply
I_{D}	A	MOSFET drain dc OP current
$I_{\text{ED,OP}}$	A	energy detector (ED) dc OP current
I_{FB}	A	feedback current
I_{leak}	A	leakage current when turned off
I_{on}	A	current consumption when turned on
I_{s1}	A	SRA signal amplitude term under bit 1 reception
IC	1	inversion coefficient (IC) of a MOSFET
k_{ED}	1/V	ED conversion gain
L	m	gate length of a MOSFET
L_1	H	motional inductance of the SAW resonator BVD model
L_2	H	off-chip parallel inductor of the SPIN
L_{2T}	H	top half of split off-chip parallel inductor of the SPIN
L_{2B}	H	bottom half of split off-chip parallel inductor of the SPIN
L_{antenna}	m	geometrical length of an antenna
$L_{\text{att,dB}}$	dB	additional attenuation/losses in a wireless transmission system
N_{max}	1	N_{max}-th maximum, $N_{\text{max}} \in \mathbb{N}$
$N_{\text{bit,code}}$	bit	length of the code or of the WUS
N_{finger}	1	number of MOSFET gate fingers
N_{X}	1	turns ratio of a transformer
P_{10}	1	10-th percentile of the distribution of an RV
P_{90}	1	90-th percentile of the distribution of an RV
P_{avg}	W	average dc power consumption
P_{dc}	W	dc power consumption
P_{in}	W or dBm	input power available from the antenna port; i.e., power delivered from the 50 Ω antenna port to a connected 50 Ω load

Symbol	Unit	Description
$P_{\text{in,ref,dBm}}$	dBm	reference input power in dB-scale
$P_{\text{in,sens}}$	W	input sensitivity (BER $\leq 10^{-3}$) in linear scale
$P_{\text{in,sens,CER,dBm}}$	dBm	input sensitivity (CER $\leq 10^{-3}$) in dB-scale
$P_{\text{in,sens,dBm}}$	dBm	input sensitivity (BER $\leq 10^{-3}$) in dB-scale
P_{noise}	W	noise power
$P_{\text{Rx,dBm}}$	dBm	receive power in dB-scale
P_{signal}	W	signal power
$P_{\text{Tx,dBm}}$	dBm	transmit power in dB-scale
PG_{dB}	dB	processing gain (PG) of a spread spectrum code in dB-scale
PLE	1	path loss exponent (PLE)
Q	1	quality factor of a resonant circuit
Q_{L2}	1	quality factor of the inductor L_2
Q_{L2C2}	1	quality factor of the L_2C_2 tank
$Q_{\text{RLC,BPF}}$	1	quality factor of the SAW resonator connected as series band-pass filter (BPF)
$Q_{\text{SAW,charge}}$	1	quality factor of the SAW resonator in the charge phase
r_{DS}	Ω	drain-source small-signal resistance
R	bps	bit rate
R_0	Ω	antenna/source resistance
R_1	Ω	motional resistance of the SAW resonator BVD model
R_{b}	Ω	bias resistor
$R_{\text{C2,stray}}$	Ω	parallel loss resistance associated with $C_{2,\text{stray}}$
R_{loss}	Ω	total parallel loss resistance of the SPIN
R_{L}	Ω	load resistance
R_{L2}	Ω	inductor L_2 parallel loss resistance
R_{L2B}	Ω	inductor $L_{2\text{B}}$ parallel loss resistance
R_{L2C2}	Ω	total parallel resistance of the SPIN, including G_{osc}
R_{L2T}	Ω	inductor $L_{2\text{T}}$ parallel loss resistance
R_{on}	Ω	on-resistance of a MOSFET switch

Symbol	Unit	Description
R_{off}	Ω	off-resistance of a MOSFET switch
R_{source}	Ω	source resistance
R_{TV}	Ω	time-varying (TV) resistance
RB_i	1	i-th receive bit, which is a RV with Bernoulli distribution
RC_i	1	correlation of the i-th receive bit RB_i with the code bit C_i
$s_{\text{VV}}(t)$	V^2	autocorrelationfunction (ACF) of $V(t)$
$\underline{S}_{11}$	1	input reflection scattering parameter
$S_\text{I}(\omega)$	A^2/Hz	double-sided power spectral density (PSD) of noise current $I(t)$
$S_\text{I}(\omega,t)$	A^2/Hz	TV double-sided PSD of noise current $I(t)$
$S_{\text{I}'}(\omega,t)$	A^2/Hz	TV double-sided PSD of noise current time derivative $\frac{d}{dt}I(t)$
S_{I1}	A^2/Hz	white noise current double-sided PSD during phase 1
S_{I2}	A^2/Hz	white noise current double-sided PSD during phase 2
$S_{\text{ID}}(\omega)$	A^2/Hz	double-sided PSD of MOSFET thermal drain noise current
$S_{\text{I,R}}(\omega)$	A^2/Hz	double-sided PSD of noise current source associated with resistor R
$S_\text{V}(\omega)$	V^2/Hz	double-sided PSD of noise voltage $V(t)$
SIR	dB	signal-to-interference ratio (SIR)
SNR	1	signal-to-noise ratio (SNR) in linear scale
SNR_dB	dB	SNR in dB-scale
SNR_input	dB	input SNR
SNR_output	dB	output SNR
SNR_ref	1	SNR in linear scale for reference input power $P_{\text{in,ref}}$
t	s	time
$\tilde{t}$	s	independent time variable used in integrals
t_0	s	transition time from phase 1 to phase 2; SITO: time, when antenna switch opens
t_1	s	start time of phase 1

Symbol	Unit	Description
t_2	s	stop time of phase 2
t_b	s	ramp length of a ramp controlled SRR
t_bit	s	period length of received bit
t_latency	s	latency of WUS reception
t_on	s	on-time of the receive chain or oscillator
t_sample	s	sampling point in time of the SITO Rx
t_settle	s	turn-on settling time of the receive chain or oscillator
t_up	s	ramp-up time of an SRA
t_x	s	constant offset time
t_y	s	constant offset time
T	K	temperature
T_win	s	window length of Fourier transform $V_\mathrm{T,win}(\omega)$
$T_{90\,\%}$	s	90 % settling time
TE	1/V	transistor efficiency (TE) of a MOSFET
u	rad/s	independent angular frequency variable used in integrals
$\hat{V}$	V	amplitude of sinusoidal voltage V
$V(t)$	V	a noise voltage
$\overline{V^2}$	V^2	mean square (MS) of noise voltage $V(t)$
V_A	V	voltage of node A referred to ground
V_b	V	bias voltage
$V_\mathrm{b,ED}$	V	ED bias voltage
$V_\mathrm{b,osc}$	V	oscillator bias voltage
V_C1	V	voltage across C_1
V_DAC	V	DAC output voltage
V_DD	V	supply voltage
$V_\mathrm{ED,buf}$	V	ED buffer output voltage
$V_\mathrm{ED,in}$	V	ED input voltage
$V_\mathrm{ED,in,n}$	V	ED input noise voltage
$V_\mathrm{ED,in,UG}$	V	ED input unity gain (UG) point voltage
$V_\mathrm{ED,out}$	V	ED output voltage
$V_\mathrm{ED,out,dc-shift}$	V	dc shift of the ED output voltage

Symbol	Unit	Description
$V_{\mathrm{ED,out,n}}$	V	ED negative output voltage
$V_{\mathrm{ED,out,NN}}$	V	noise-noise mixing term of ED output voltage
$V_{\mathrm{ED,out,p}}$	V	ED positive output voltage
$V_{\mathrm{ED,out,SN}}$	V	signal-noise mixing term of ED output voltage
$V_{\mathrm{ED,out,SS}}$	V	signal-signal mixing term of ED output voltage
$\hat{V}_{\mathrm{f1}}$	V	amplitude of sinusoidal f_1 component of voltage V
$\hat{V}_{\mathrm{f2}}$	V	amplitude of sinusoidal f_2 component of voltage V
V_{GS}	V	gate-source voltage
V_{L}	V	load voltage across R_{L}
$V_{\mathrm{LNA,out}}$	V	low noise amplifier (LNA) output voltage
V_{n}	V	negative voltage
$V_{\mathrm{noise}}(t)$	V	a noise voltage
V_{osc}	V	output voltage of first OTA stage of two stage one-port oscillator
$V_{\mathrm{osc,buf}}$	V	oscillator buffer output voltage
$V_{\mathrm{osc,out}}$	V	oscillator output voltage
$\hat{V}_{\mathrm{osc,UG}}$	V	UG point of ED input voltage, which is oscillator output voltage
V_{out}	V	output voltage
V_{p}	V	positive voltage
$V_{\mathrm{sig}}(t)$	V	a signal voltage
$\underline{V_{\mathrm{sig}}}$	V	complex phasor of the signal voltage
$V_{\mathrm{sig,thresh}}$	V	threshold for OOK demodulation of $V_{\mathrm{sig}}(t)$
V_{source}	V	open-load voltage of the antenna port or source port
$V_{\mathrm{SAW}}(t)$	V	voltage across the SAW resonator and thus across C_2
$\hat{V}_{\mathrm{SAW}}(t)$	V	instantaneous amplitude of single-tone signal $V_{\mathrm{SAW}}(t)$
$V_{\mathrm{SAW,bit0}}(t)$	V	envelope of $V_{\mathrm{SAW}}(t)$ for bit 0 reception

Symbol	Unit	Description
$V_{\mathrm{SAW,env}}(t)$	V	envelope of $V_{\mathrm{SAW}}(t)$
$V_{\mathrm{SAW,f1}}(t)$	V	sinusoidal f_1 component of voltage $V_{\mathrm{SAW}}(t)$
$\hat{V}_{\mathrm{SAW,f1}}(t)$	V	instantaneous amplitude of $V_{\mathrm{SAW,f1}}(t)$
$V_{\mathrm{SAW,f2}}(t)$	V	sinusoidal f_2 component of voltage $V_{\mathrm{SAW}}(t)$
$\hat{V}_{\mathrm{SAW,f2}}(t)$	V	instantaneous amplitude of $V_{\mathrm{SAW,f2}}(t)$
V_{SW}	V	antenna switch control voltage
V_{tail}	V	tail bias voltage of a differential pair
V_{th}	V	threshold voltage of MOSFET
$V_{\mathrm{thresh,BB}}$	V	threshold voltage in the BB associated with the comparator input voltage
$V_{\mathrm{thresh,SAW}}$	V	threshold voltage associated with $V_{\mathrm{SAW}}(t)$
V_{T}	V	thermal voltage
$V_{\mathrm{T,win}}(\omega)$	s	Fourier transform of the signal $V(t)$ windowed over time T_{win}
W	m	gate width of a MOSFET
$x(t)$	A/s	SRA injection term
$x_1(t)$	A/s	$x(t)$ during phase 1
$x_2(t)$	A/s	$x(t)$ during phase 2
$\underline{X}(\omega)$	A	Fourier transform of $x(t)$
$\angle\underline{X}(\omega)$	rad	phase of $\underline{X}(\omega)$
$\underline{X_1}(\omega)$	A	Fourier transform of $x_1(t)$
$\underline{X_2}(\omega)$	A	Fourier transform of $x_2(t)$
$\underline{Y}(j\omega)$	S	admittance $\underline{Y}(j\omega) = 1/\underline{Z}(j\omega)$
$\underline{Y}(\omega_1)$	A	SITO signal term including noise
$\underline{Y}(\omega_2)$	A	SITO signal term including noise
$\underline{Y}_1(j\omega)$	S	admittance of the SAW resonator branch
$\underline{Y}_2(j\omega)$	S	admittance of the parallel L_2C_2 tank
$\underline{Y}_{\mathrm{osc}}(j\omega)$	S	admittance of the oscillator active element (AE)
$\underline{Y}_{\mathrm{total}}(j\omega)$	S	total admittance of the SPIN
$\underline{Z}(j\omega)$	Ω	impedance
Z_0	Ω	characteristic impedance of a resonator
$\underline{Z}_1$	Ω	impedance of the SAW resonator branch
$\underline{Z}_{11}$	Ω	input impedance

Symbol	Unit	Description
Z_{f1}	Ω	characteristic impedance of the SPIN at frequency f_1
Z_{f2}	Ω	characteristic impedance of the SPIN at frequency f_2
$\underline{Z}_{\mathrm{GS}}$	Ω	gate-source impedance
$\underline{Z}_{\mathrm{in}}$	Ω	input impedance
$\underline{Z}_{\mathrm{out1}}$	Ω	impedance of the output node V_{osc} of first OTA stage against ground
$\underline{Z}_{\mathrm{SAW}}$	Ω	input impedance of voltage V_{SAW} to ground as seen from the antenna switch

Notation Conventions

Citations

Other work is referenced by a number in square brackets, e.g., [3]. Own citations contain the prefix "Mel" and a number in square brackets, e.g., [Mel1]. A reference to a specific figure or section might be added within square brackets. e.g., [Mel1, Fig. 1] or [Mel1, section II].

Literal citations are written in quotes, with the reference following, e.g., "Lorem ipsum" [3]. Changes to text passages or omissions within literal citations (without changing the semantics) are denoted by curly brackets, e.g., "{lorem} ipsum dolor {...} amet" [3].

Equation References

Equations are references to by their number in round brackets, e.g., see (1):

$$\sqrt{-1} = \pm j\,. \tag{1}$$

Previous Publications

This thesis contains content, which was previously published by the same first author in [Mel1], [Mel2], [Mel3], [Mel4], [Mel5] and [Mel6]. These works are listed in the bibliography section under "own publications". Literal citations and adoption of figures or tables from the above publications are indicated by the citation reference and a copyright note of the copyright holder with the year of publication.

[1] was co-authored by the author of this work.

The author contributed to [2].

Contents

1 Introduction

1.1 Motivation

The electrical power consumption of Germany's cellular network is growing by a factor of 2.9 within 10 years [4], where the same trend will be observable on a global scale. Furthermore [4] reports, that more than 90 % of this energy is consumed by the hardware over its operating lifetime, as opposed to the energy required to manufacture the hardware. The increase in wireless data throughput over the years cannot be compensated by current advancements in hardware efficiency, resulting in an ever increasing demand for energy [5].

With an expected number of 10^{12} internet of things (IoT) devices by the year 2035 [6] and a current annual growth rate of this number of 22 % [7], IoT will consume a significant part of the energy expended for information and communications technology (ICT). If all these IoT end nodes were battery powered, a huge number of batteries would be required [7], leading to massive resource costs and huge maintenance effort [8]. The above growth in IoT deployment can only be enabled, if the battery problem can be overcome [8]. Specifically it is required, that the wireless node either can be powered by a single battery over its entire life time or, even better, it can be powered by harvested energy, eliminating the need for batteries at all.

Wakeup receivers (WuRxs) pose a possible solution to this problem, as they can synchronize data transmission between nodes of a wireless network and, thus, can greatly reduce the average power consumption of these [9]. A WuRx hardware can handle two different tasks:

1. waking up a wireless node or a different analog frontend (AFE)
2. receiving payload data with low bit rates, e.g., below 100 kbps, while consuming only very little direct current (dc) power, e.g., below 10 µW.

Consequently, three possible fields of application of WuRxs are:

1. 6G mobile communications gearbox-PHY [10], [11]: a WuRx can wake up a high data rate AFE with a high dc power consumption in a mobile communication system, or provide a low data rate gear itself
2. IoT: wireless nodes that are rarely wirelessly polled, e.g., once an hour
3. wireless sensor networks: distributed sensor mesh networks, which demand low maintenance and long node lifetime.

The latter two applications can benefit from low power WuRxs in several possible ways, according to M. Methfessel (IHP, Frankfurt (Oder), Germany; personal communication, Feb. 2, 2025):

1. on-demand data collection: sensor nodes store data locally until read out from a nearby device or gateway, thus minimizing power consumption.
2. remote command: end nodes are in standby mode while maintaining permanent accessibility, enabling remote controllability for increased monitoring activity during alerts or temporary activation of an actuator.
3. swarm intelligence: sensor nodes communicate and analyze data collectively, enabling real-time monitoring and reducing the need for central processing.
4. multi-hop networks: sensor nodes can relay data via multiple hops in large scale networks.

Accordingly, energy efficient WuRxs open up a wide range of applications, which rely on status monitoring using distributed sensor networks. These sensor networks typically contain many nodes and often need to cover large areas. Possible applications of such distributed wireless sensor networks are:

1. monitoring of soil composition, temperature or humidity in agriculture or composting plants
2. pest and fire monitoring in forests
3. wildlife observation
4. monitoring of cargo train wagons, e.g., reporting derailment of single wagons
5. filling status monitoring of containers in cargo harbors
6. structural health monitoring, e.g., of bridges [12] [13] [14], buildings and wind turbines.

1.2 Specifications

The main task of a WuRx is to receive a wakeup sequence (WUS) with little latency, while consuming only little power from the dc supply and at the same time providing a proper input sensitivity for sufficient transmission distance [9]. The required latency t_{latency} is typically in the range of $t_{\mathrm{latency}} \in [10\,\mathrm{ms}, 10\,\mathrm{s}]$. The WUS to be received is usually several tens of bits long, e.g., 31 (see [15, section 3.9]). Oversampling by a factor of at least 2 allows for unsynchronized sampling of the received signal [15, section 3.1.2]. Two-times oversampling is applied in this work. According to the latency requirement

t_{latency} and the length $N_{\text{bit,code}}$ of the WUS (also referred to as *code* in this work) including oversampling, the required bit rate R can be deduced:

$$R \geq \frac{N_{\text{bit,code}}}{t_{\text{latency}}}\,. \tag{1.1}$$

In this work, the term *bit* refers to a single sample obtained by the receiver (Rx) AFE. Accordingly, bit rate R and sampling frequency f_{sampling} are considered the same. Table 1.1 lists the main specifications used as a baseline for the WuRx designs discussed in this work. In conjunction with a proper input

System Parameter	Symbol	Specification
input frequency	f_{in}	$\in [433.05\,\text{MHz}, 434.79\,\text{MHz}]$
input sensitivity (BER $\leq 10^{-3}$)	$P_{\text{in,sens,dBm}}$	$\leq -90\,\text{dBm}$
latency	t_{latency}	$\in [10\,\text{ms}, 10\,\text{s}]$
wakeup sequence length	$N_{\text{bit,code}}$	$= 62$
bit rate	R	$\in [10\,\text{bps}, 100\,\text{kbps}]$
dc power consumption	P_{dc}	$\leq 10\,\mu\text{W}$
supply voltage	V_{DD}	$\leq 1.5\,\text{V}$

Table 1.1: WuRx specifications relevant for this work.

sensitivity $P_{\text{in,sens,dBm}} \leq -90\,\text{dBm}$ (BER $\leq 10^{-3}$), a sub-GHz industrial, scientific and medical (ISM) band is suitable for sufficient transmission distances, as will be discussed in section 2.

1.3 State of the Art Receiver Architectures

An overview of state-of-the-art (SOTA) low power Rx architectures is given in [16] and [17]. These Rx architectures can basically be divided into frequency conversion Rxs, direct radio frequency (RF) demodulation Rxs and super-regenerative receivers (SRRs), as outlined below.

1.3.1 Frequency Conversion Receivers

The super-heterodyne Rx [18, section 4.2.1] generically depicted in Fig. 1.1 is the most conventional architecture of a wireless Rx. An input matching network (IMN) matches the input impedance of the receiver (Rx) to the antenna impedance, which is typically $50\,\Omega$. Gain at RF is provided by a low noise amplifier (LNA). The LNA is typically a power-hungry block, which is

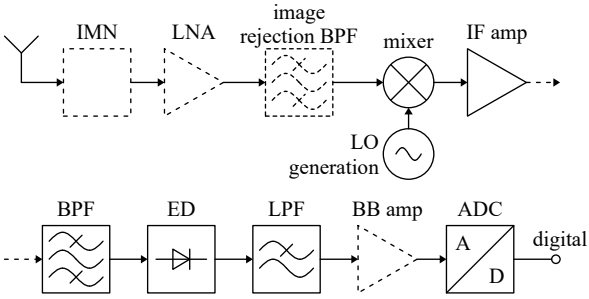

Figure 1.1: Generic block diagram of a super-heterodyne Rx. Based on [17, Fig. 1(c)].

why it might be omitted in a low power Rx design. A band-pass filter (BPF) improves image rejection beyond the frequency selectivity of the IMN. A mixer shifts the RF frequency of the input signal down to an intermediate frequency (IF) by means of a local oscillator (LO) signal. The mixer could be either active, potentially providing a rather large conversion gain, or passive. For amplitude-shift keying (ASK) demodulation, the IF signal is converted to baseband (BB) with an energy detector (ED), followed by a low-pass filter (LPF). After an optional BB amplifier, the signal is digitized by an analog-to-digital converter (ADC), which can be a comparator in the most simple case. The Rx chain depicted in Fig. 1.1 can only demodulate incoherently, i.e., ASK modulated signals (on-off keying (OOK) modulated signals in the simplest case). If coherent signal demodulation is desired, quadrature (Q-) LO signal generation, mixer and BB paths would need to be added in addition to the existing in-phase (I-) path. Due to this increase in system complexity, IQ-demodulation is usually not implemented in low power Rxs.

The tone for frequency down conversion (i.e., mixing) is typically generated locally by a voltage-controlled oscillator (VCO), hence the name *LO signal*. This Rx variant is also referred to as "on-chip LO" Rx in [17]. A phase-locked loop (PLL) employs a stable reference oscillator in order to control the VCO frequency, thus stabilizing the VCO frequency and reducing the phase noise (PN) of the VCO output signal. However, a PLL is a rather complex sub-system with significant dc power consumption. It is unsuited for bit-level duty-cycling (BLDC) (see section 3.2), since a rather long time is required to achieve phase lock.

A huge advantage of the super-heterodyne Rx architecture over the direct RF demodulation Rx (discussed below) is, that channel filtering by the BPF in the IF can be comparatively narrowband. On the other hand, RF filters

exhibit a much larger absolute filter bandwidth (BW), due to the high RF frequency compared to the IF and due to the limited quality factor of the filter. Still, RF band-pass filtering is required in a super-heterodyne Rx to suppress image frequencies in the mixing process [18, p. 161 ff.].

As an alternative to a locally generated LO signal, the tone for frequency down conversion could also be sent by the transmitter (Tx) in addition to the original transmit signal. The Rx then performs self-mixing of the input signal and, hence, down conversion in an ED. This is referred to as "transmitted LO scheme" in [17]. The so-called LO signal of the Rx is actually a misnomer in this case, since this signal is not generated *locally* in the Rx, but in the Tx instead.

1.3.2 Direct RF Demodulation Receivers

A direct RF demodulation Rx assesses the received signal energy contained in the desired frequency band. Since it is an incoherent Rx, it cannot extract the RF phase from the signal. Hence, this architecture is suited only for the reception of ASK modulated signals. A generic block diagram of a direct RF demodulation Rx is given in Fig. 1.2. Similar to the super-heterodyne Rx

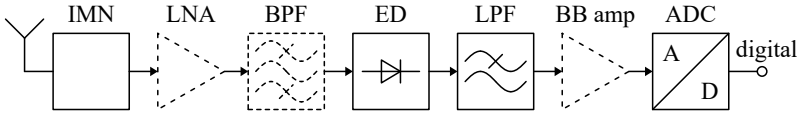

Figure 1.2: Direct RF detection Rx. Based on [17, Fig. 1(a)].

(section 1.3.1), the 50 Ω antenna is interfaced by an input matching network (IMN) and an LNA. The ED mixes the signal with itself, by exploiting the second order non-linearity of its transfer characteristic. A BPF in front of the ED aids in suppression of undesired interferers and noise, which enter the ED and both are mixed down to the BB at the ED output (see section 5.2). The following LPF suppresses higher mixing products of the ED output signal. A BB amplifier might be included for sufficient voltage swing at the ADC input.

The main benefits of the direct RF demodulation Rx compared to the super-heterodyne Rx are the simplified architecture and the elimination of LO signal generation.

1.3.3 Super-Regenerative Receiver

An SRR [19], [20], [21] is based on a super-regenerative amplifier (SRA), as shown in Fig. 1.3 (component names align with chapter 6). An SRA

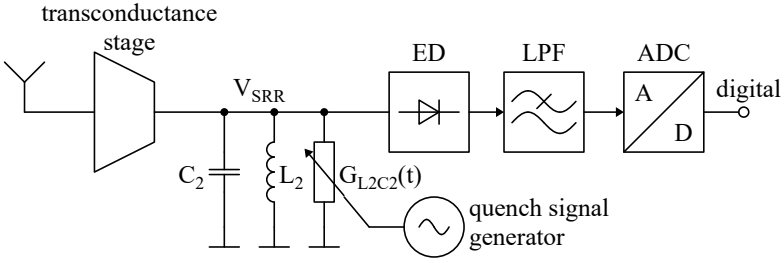

Figure 1.3: Basic schematic of an SRR consisting of an quenched oscillator and a BB signal chain. Based on [Mel1, Fig. 2] ©2024 IEEE.

is a switched or quenched oscillator with a signal injection path via a transconductance stage. The transconductance stage can be either active, e.g., an operational transconductance amplifier (OTA) or passive, e.g., an input matching network (IMN) or a transformer. The SRA can provide a large super-regenerative gain over time from a comparatively low small-signal gain of the active element in its dc operating point (OP) [22] [23]. The parallel oscillator conductance $G_{\mathrm{L2C2}}(t)$ is controlled by a quench signal. If this signal is a linear ramp resulting in a linear ramp of the damping ratio, then the SRR is called *ramp controlled*. The RF phase of the input signal is retained after amplification by the SRA, enabling coherent signal reception [24]. In favor of the simplicity of the Rx and of a low dc power consumption, usually an ED (see Fig. 1.3) is used for incoherent signal demodulation.

The SRA concept can also be used, e.g., for active reflector tags [22].

1.4 Receiver Architectures Proposed in This Work

1.4.1 Switched Passive Input Network Amplifier Receiver

The switched passive input network (SPIN) amplifier Rx shown in Fig. 1.4 is basically a direct RF demodulation Rx with the main difference, that the IMN in steady-state operation is replaced by a SPIN based on a surface acoustic wave (SAW) resonator (the SPIN will be introduced in chapter 4). This Rx architecture will be discussed in chapter 5.

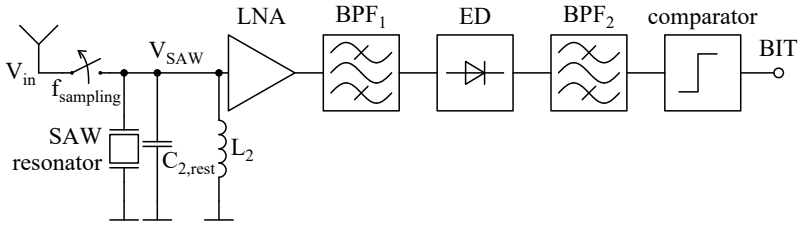

Figure 1.4: Schematic of the SPIN amplifier Rx.

1.4.2 Switched Injection-Triggered Oscillator Receiver

The switched injection-triggered oscillator (SITO) Rx as shown in Fig. 1.5 is an alteration of the SRR, where the RF signal is not injected into the oscillator by a transconductance stage as shown in Fig. 1.3, but by means of a switched SAW resonator. The switched SAW resonator is part of the

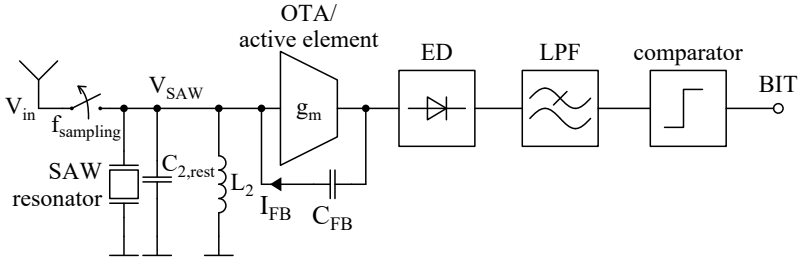

Figure 1.5: Schematic of the SITO Rx.

very same SPIN also used in the SPIN amplifier Rx above. The SITO Rx will be discussed in detail in chapter 6. SRR and SITO Rx will be compared to each other in chapter 7.

1.4.3 Classification

The two mentioned Rx architectures, which are the focus of this work, are classified in the context of the SOTA Rx architectures (listed in section 1.3) in Fig. 1.6.

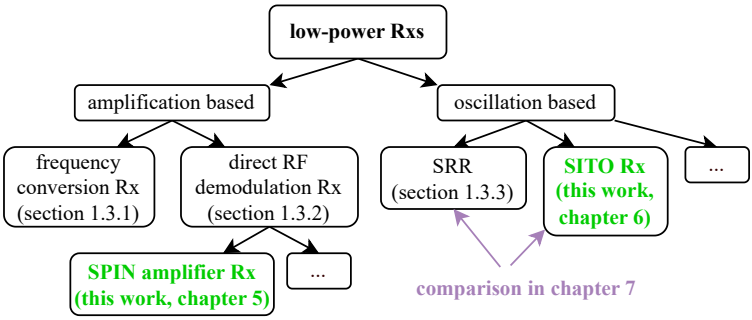

Figure 1.6: Classification of the SPIN amplifier Rx (chapter 5) and SITO Rx (chapter 6) proposed in this work.

1.5 Research Theses

These are the main research theses, which will be discussed throughout this work:

1. The most important metrics of a WuRx are carrier frequency, consumed dc energy per bit, input sensitivity, bit rate and frequency selectivity.
2. A switched passive input network (SPIN) consisting of a SAW resonator in conjunction with an antenna switch is able to perform passive signal filtering and amplification to a high degree.
3. The SPIN readout phase, where energy from the dc supply is consumed, can be comparatively short, which aids in minimizing the BLDC ratio and hence minimizing the average dc power consumption of the Rx.
4. The SPIN fed with a single tone continuous wave (CW) signal in the charge phase yields a two tone signal in the discharge phase.
5. The SPIN enables two different AFE types, which both show high performance in measurements compared to the SOTA: the SPIN amplifier Rx and the SITO Rx.
6. A proof-of-concept SPIN amplifier Rx was successfully tested in an outdoor environment over a distance of 115 m.
7. A superposition of two separate oscillation modes can be used to model the signal and noise behavior of the SITO Rx, based on existing noise theory of the single resonator SRR.
8. The SITO Rx behaves contrary to a ramp controlled SRR with respect to input sensitivity vs. time domain expansion of the ramp-up.
9. The input frequency selectivity of the SITO Rx is dominantly given by the SAW resonator and is consequently largely independent of the time domain expansion of the ramp-up. In contrast, the SRR requires

a ramp-up stretched over a long time in order to achieve a comparably narrow input 3dB BW.
10. The resulting WuRx AFEs can be powered by energy harvesting, which has been confirmed in experiments.
11. A SITO Rx can improve the energy efficiency compared to SOTA low power Rxs by a factor of more than 130.

1.6 Structure of this Dissertation

First, fundamental wireless Rx design considerations are discussed in chapter 2. Techniques and challenges specifically regarding low power Rx design are discussed in chapter 3. Chapter 4 gives a general introduction to the SPIN based on a SAW resonator, which enables basically two different Rx AFE types:

1. the SPIN amplifier Rx as discussed in chapter 5
2. the SITO Rx presented and analyzed in chapter 6.

A comparison between SITO Rx and SRR is given in chapter 7. The low dc power consumption of the presented WuRxs enables operation from energy harvesting devices, as shown in chapter 8. A wireless transmission outdoor experiment is described in chapter 9. Finally, the results are summarized in chapter 10 and an outlook is given in chapter 11.